A first-in-class Wiskott-Aldrich syndrome protein activator with antitumor activity in hematologic cancers

Filippo Spriano,[1+] Giulio Sartori,[1] Jacopo Sgrignani,[2] Laura Barnabei,[1] Alberto J. Arribas,[1,3] Matilde Guala,[4] Ana Maria Carrasco Del Amor,[5] Meagan R. Tomasso,[6] Chiara Tarantelli,[1] Luciano Cascione,[1,3] Gaetanina Golino,[1,7] Maria E. Riveiro,[8] Roberta Bortolozzi,[9,10] Antonio Lupia,[7,11] Francesco Paduano,[12,13] Samuel Huguet,[14] Keyvan Rezai,[14] Andrea Rinaldi,[1] Francesco Margheriti,[1] Pedro Ventura,[2] Greta Guarda,[2] Giosuè Costa,[12] Roberta Rocca,[12] Alberto Furlan,[2] Luuk M. Verdonk,[15] Paolo Innocenti,[15] Nathaniel I. Martin,[15] Giampietro Viola,[9,10] Christoph Driessen,[16] Emanuele Zucca,[1,17] Anastasios Stathis,[17] Digvijay Gahtory,[18] Maurits van den Nieuwboer,[18] Beat Bornhauser,[19] Stefano Alcaro,[12] Francesco Trapasso,[12] Susana Cristobal,[5,20] Shae B. Padrick,[6] Natalina Pazzi,[4] Franco Cavalli,[1] Andrea Cavalli,[2] Eugenio Gaudio[1+] and Francesco Bertoni[1,17]

[1]Institute of Oncology Research, Faculty of Biomedical Sciences, USI, Bellinzona, Switzerland; [2]Institute of Research in Biomedicine, Faculty of Biomedical Sciences, USI, Bellinzona, Switzerland; [3]SIB Swiss Institute of Bioinformatics, Lausanne, Switzerland; [4]Chimete, Tortona, Italy; [5]Department of Biomedical and Clinical Sciences, Cell Biology, Medical Faculty, Linköping University, Linköping, Sweden; [6]Drexel University, College of Medicine, Department of Biochemistry and Molecular Biology, Philadelphia, PA, USA; [7]Department of Pharmacy, University of Napoli Federico II, Napoli, Italy; [8]Early Drug Development Group, Boulogne-Billancourt, France; [9]Department of Woman's and Child's Health, University of Padova, Padova, Italy; [10]Istituto di Ricerca Pediatrica IRP, Fondazione Città della Speranza, Padova, Italy; [11]Net4science Srl, Magna Graecia University of Catanzaro, Catanzaro, Italy; [12]University "Magna Græcia" of Catanzaro, Catanzaro, Italy; [13]Tecnologica Research Institute and Marrelli Health, Biomedical Section, Stem Cells and Medical Genetics Units, Crotone, Italy; [14]Institut Curie, Paris, France; [15]Biological Chemistry Group, Institute of Biology Leiden, Leiden University, Leiden, the Netherlands; [16]Kantosspital St Gallen, St Gallen, Switzerland; [17]Oncology Institute of Southern Switzerland, Ente Ospedaliero Cantonale, Bellinzona, Switzerland; [18]BIMINI Biotech B.V., Leiden, the Netherlands; [19]Children's Hospital Zurich, Zurich, Switzerland; [20]Ikerbasque, Basque Foundation for Sciences, Department of Physiology, Faculty of Medicine and Nursing, University of the Basque Country, Bilbao, Spain

[+]*FS and EG contributed equally to this work.*

Correspondence: E. Gaudio
eugaudio1976@gmail.com

F. Bertoni
francesco.bertoni@ior.usi.ch

Received: December 31, 2022.
Accepted: June 7, 2024.
Early view: June 20, 2024.

https://doi.org/10.3324/haematol.2022.282672

A first-in-class Wiskott-Aldrich syndrome protein activator with anti-tumor activity in hematological cancers

Filippo Spriano [1*], Giulio Sartori [1], Jacopo Sgrignani [2], Laura Barnabei [1], Alberto J. Arribas [1,3], Matilde Guala [4], Ana Maria Carrasco Del Amor [5], Meagan R. Tomasso [6], Chiara Tarantelli [1], Luciano Cascione [1,3], Gaetanina Golino [1,7], Maria E Riveiro [8], Roberta Bortolozzi [9,10], Antonio Lupia [7,11], Francesco Paduano [12,13], Samuel Huguet [14], Keyvan Rezai [14], Andrea Rinaldi [1], Francesco Margheriti [1], Pedro Ventura[2], Greta Guarda [2], Giosuè Costa [12], Roberta Rocca [12], Alberto Furlan [2], Luuk M. Verdonk [15], Paolo Innocenti [15], Nathaniel I. Martin [15], Giampietro Viola [9,10], Christoph Driessen [16], Emanuele Zucca [1,17], Anastasios Stathis [17], Digvijay Gahtory [18], Maurits van den Nieuwboer [18], Beat Bornhauser [19], Stefano Alcaro [12], Francesco Trapasso [12], Susana Cristobal [5,20], Shae B. Padrick [6], Natalina Pazzi [4], Franco Cavalli [1], Andrea Cavalli [2], Eugenio Gaudio [1*#], Francesco Bertoni [1,17#],

[1] Institute of Oncology Research, Faculty of Biomedical Sciences, USI, Bellinzona, Switzerland; [2]Institute of Research in Biomedicine, Faculty of Biomedical Sciences, USI, Bellinzona, Switzerland; [3] SIB Swiss Institute of Bioinformatics, Lausanne, Switzerland;[4] Chimete, Tortona, Italy; [5] Department of Biomedical and Clinical Sciences, Cell Biology, Medical Faculty, Linköping University, Linköping, Sweden; [6] Drexel University, College of Medicine, Department of Biochemistry and Molecular Biology, Philadelphia, PA, USA; [7]Department of Pharmacy, University of Napoli Federico II, Napoli, Italy; [8] Early Drug Development Group, Boulogne-Billancourt, France; [9]Department of Woman's and Child's Health, University of Padova, Italy; [10] Istituto di Ricerca Pediatrica IRP, Fondazione Città della Speranza, Padova, Italy; [11] Net4science Srl, Magna Graecia University of Catanzaro, Catanzaro, Italy; [21] University "Magna Græcia" of Catanzaro, Catanzaro, Italy; [13] *Tecnologica Research Institute and Marrelli Health, Biomedical Section, Stem Cells and Medical Genetics Units, Crotone, Italy. [14] Institut Curie, Paris, France; [15] Biological Chemistry Group, Institute of Biology Leiden, Leiden University, Leiden, The Netherlands; [16] Kantosspital St Gallen, St Gallen, Switzerland; [17] Oncology Institute of Southern Switzerland, Ente Ospedaliero Cantonale, Bellinzona, Switzerland; [18] BIMINI Biotech B.V., Leiden, The Netherlands; [19] Children's Hospital Zurich, Zurich, Switzerland; [20] Ikerbasque, Basque Foundation for Sciences, Department of Department of Physiology, Faculty of Medicine and Nursing, University of the Basque Country, Spain.*

*, equally contributed; #, co-corresponding authors

Supplementary materials

Supplementary materials and methods

Solid tumor and leukemia cell lines

Cell lines derived from solid tumors (Supplementary Figure 2) were obtained from the American Type Culture Collection (ATCC; Rockville, MD, USA). Cells were cultured in RPMI 1640 with L-glutamine medium (Gibco, ThermoFisher Scientific Inc., Waltham, MA, USA) supplemented with 10% FBS (#26140079, Gibco FBS qualified USA origin, Life Technologies, Saint Aubin, France), 2 mM glutamine (PAA Laboratories, Velizy-Villacoublay, France), 100 units/ml penicillin and 100 µg/ml streptomycin (PAA Laboratories). MCF7 cells were cultured in MEM Eagle (ATCC; Rockville, MD, USA) supplemented with 0.01mg/ml human recombinant insulin (Sigma-Aldrich, France), 10% FBS (#26140079, Gibco FBS qualified USA origin, Life Technologies, Saint Aubin, France), 2 mM glutamine (PAA Laboratories, Velizy-Villacoublay, France), 100 units/ml penicillin and 100 µg/ml streptomycin (PAA Laboratories). Cells lines were cultured at 37°C in a humidified 5% CO_2 atmosphere. Cell lines with a passage number in the range between 5 and 40 were maintained in culture for a maximum of 6 weeks.

Seven T-cell acute lymphoblastic leukemia (ALL), two B-cell ALL, one promyelocytic leukemia and one medulloblastoma cell lines were cultured in RPMI-1640 medium (Gibco, US). Medulloblastoma cell line DAOY was grown in MEMalpha, and the colon cancer cell line HT29 in DMEM. Cell culture media were supplemented with fetal bovine serum (10%) (Gibco, US), Penicillin-Streptomycin (10,000 U/mL) (1%) (Gibco, US), and L-glutamine (1%) (Gibco, US). All cell lines were purchased from ATCC, and all the experiments were performed within 1 month of being thawed and periodically tested for Mycoplasma negativity.

MTT proliferation assay

Lymphoma and solid tumor cell lines were exposed to a large range of concentrations of EG-011 as a single agent for 72h, followed by MTT and, after 4h, SDS to stop the reaction. The day after, plates were read using a Cytation 3 multimode plate reader (Biotek), and IC_{50}s were calculated. IC_{50} was defined as the drug concentration that gave 50% of proliferating cells compared to vehicle-treated cells. Lymphoma cell lines with IC_{50} below 1µM were considered sensitive to the treatment. The area under the curve (AUC) was calculated with GraphPad. Cell viability of twelve acute lymphoblastic leukemia (ALL) primary patient cells from different high-risk subgroups (VNN2+, E2A-HLF, refractory T, and IKZF plus) co-culture with marrow–derived MSCs were assayed after 72h of incubation with EG-011 and controls.

Cell cycle and Apoptosis assay

For cell cycle evaluation, cell lines were fixed in cold 70% ethanol and stained with propidium iodide (PI) (Sigma Aldrich, US). Cells were analyzed by FACS, and percentages of cells in G1, S and G2/M phases of the cell cycle were determined using the FlowJo software (TreeStar Inc., Ashland, USA).

Apoptosis was evaluated through Annexin V assay (AnnexinV-FITC apop kit, Invitrogen, US). Briefly, cells were harvested, washed with PBS, and stained with Annexin V (AV) and subsequently with propidium iodide (PI). Cells AV positive/PI negative or AV positive/ PI positive were considered as apoptotic cells.

Drug combinations

OCI-LY-1, OCI-LY-8, REC1, MINO, and TMD8 cell lines were exposed (72 h) to increasing doses of EG-011 alone or in combination with increasing doses of FDA approved compounds (Rituximab, bendamustine, Ibrutinib, lenalidomide and ABT-199), followed by MTT assay. Synergism was calculated using the Chou-Talalay combination index (CI) and the MuSyC algorithm [1, 2]. CI values are referred to as median CIs for all the different combinations: additive effect (CI 0.9-1.1), synergism (CI 0.3-0.9), strong synergism (CI<0.3), and antagonism/no benefit (CI > 1.1). Efficacy values are calculated for every different concentration combination of the two drugs. Potency is calculated on IC50s and one value for each curve is obtained. Concentrations that already gave 10% or less of proliferation with the single agent were discarded for further analyses.

Patient-derived xenografts

Drug responses in ALL patient-derived xenografts (PDX) were analyzed as previously described [3]. Primary PDX were cultured on mesenchymal stroma cells, and drugs were added in serial concentrations. Cell viabilities were assessed by microscopy on an ImageXpress Micro microscope (Molecular Devices) after staining with CyQuant (Life Technologies, Thermo Fisher Scientific). Data were normalized against DMSO-treated controls, using a 4-parameter log-logistic function (R package drc [4]).

Xenografts experiments

NOD-Scid (NOD.CB17-*Prkdcscid*/NCrHsd) mice were purchased from Harlan Laboratory (five-six weeks of age, approximately 20 g body weight). Mice maintenance and animal experiments were performed under institutional guidelines established for the animal facility and with study protocols approved by the local Cantonal Veterinary Authority (No. TI-20-2015). Mice were engrafted with the MCL REC1 cell line ($15x10^6$

cells in 100 μL of PBS). Starting with tumors of 180 mm^3 volume as average, mice underwent two weeks of treatment with: EG-011 (200 mg/kg, IP, 5 days per week, no.= 9 mice), control (vehicle, ip, no.= 8 mice). EG-011 was dissolved in 25% hydroxypropyl beta cyclodextrin (HP-ß-CD) in water and adjusted at pH 6.0 using NaOH (0.1 N) and HCl (0.1 N) for *in vivo* experiments. Application volume was 4,5 mL/kg (100 mg in 4.5 mL), and mice received 200 microliters (corresponding to 200 mg/kg) though intra peritoneal i.p. injection, once per day and five days per week. Dose and schedule of EG-011 was empirically determined, since IC50s cannot provide real indication and PK data were not available.

Tumor size was measured two times per week using a digital caliper [tumor volume (mm^3) = TV=D×d2/2]. Differences in tumor volumes and weights were calculated using the Mann-Whitney test (Prism 9, Version 9.3.1). The p-value for significance was < 0.05. The Body Condition Scoring was used to assess mice health status [5].

Thermal proteome profiling (TPP)

Experiments were performed as described in Franken et al. [6] with some modifications. Cells were resuspended in ice-cold PBS. Following resuspension, cells were homogenized in vertical tip sonication at 50% and intensity at 25%, with manual cycles of 10"/5" up to a total sonication time of 3 min, before ultracentrifugation at 100,000 g for 60 min at 4 °C to collect the soluble proteome that will be analyzed by TPP. Protein concentration was determined by BCA assay [7].The soluble proteome at 1 mg/ml was incubated with the studied drug, EG-011 at 10 μM, corresponding to the recently obtained IC_{50} for this compound. The control condition following the same incubation condition with DMSO that was the vehicle solution used to solubilize the drug, The samples were incubated for 10 min at 25 ºC. For the studied EG-011, incubation was performed at the compound IC_{50}, and for the control, in the presence of the compound vehicle (DMSO). Seven aliquots of 100 μg of protein were individually heated for 3 min at different temperatures: 37 °C, 42 °C, 47 °C, 52 °C, 57 °C, 62 °C and 67 °C, followed by 3 min at room temperature. Subsequently, the samples were centrifugated at 100,000 g for 20 min at 4 °C. The supernatants were analyzed by label-free liquid chromatography-tandem mass spectrometry (nLC-MS/MS). In accordance with the TPP method [6], two biological replicates for the thermal shift assay were performed.

Filter Aided Sample Preparation (FASP)

Protein samples were prepared according to published methods [8]. First, the protein samples corresponding to the supernatants after centrifugation were prepared with SDT buffer (2% SDS, 100 mM Tris-HCl, pH 7.6 and 100 mM DTT), according to Wiśniewski et al.[8]. To perform FASP, the samples were diluted with 200 μl of 8 M urea in 0.1 M Tris/HCl, pH 8.5 (UA) in 30 kDa microcon centrifugal filter units. The filter units were centrifuged at 14,000 g for 15 min at 20 °C. The concentrated samples were diluted with 200 μl of UA and centrifuged at 14,000 g for 15 min at 20 °C. After discharging the flow-through 100 μl of 0.05 M iodoacetamide was added to the filter units, mixed for 1 min at 600 rpm on a thermo-mixer, and incubated static for 20 min in dark. The solution was drained by spinning the filter units at 14,000 g for 10 min. The filter units were washed three times with 100 μl buffer UA and centrifuged at 14,000 g for 15 min. The filter units were washed three times with 100 μl of 50 mM ammonium bicarbonate. Endopeptidase trypsin solution in the ratio 1:100 was prepared with 50 mM ammonium bicarbonate, dispensed, and mixed at 600 rpm in the thermomixer for 1 min. These units were then incubated in a wet chamber at 37 °C for about 16 h to achieve effective trypsinization. After 16 h of incubation, the filter units were transferred into new collection tubes. To recover the digested peptides, the tubes were centrifuged at 14,000 g for 10 min. Peptide recovery was completed by rinsing the filters with 50 μl of 0.5 M NaCl and collected by centrifugation. The samples were acidified with 10% formic acid (FA) to achieve pH between 3 and 2. The desalting process was performed by reverse phase chromatography in C18 top tips using acetonitrile (ACN; 60% v/v) with FA (0.1% v/v) for elution, and vacuum dried to be stored at −80 °C till further analysis.

Nano LC-MS/MS Analysis

The desalted peptides were reconstituted with 0.1% FA in ultra-pure milli-Q water and the concentration was measured using a Nanodrop (Thermo Scientific). Peptides were analyzed in a QExactive quadrupole-orbitrap mass spectrometer (Thermo Scientific). Samples were separated using an EASY nLC 1200 system (Thermo Scientific) and tryptic peptides were injected into a pre-column (Acclaim PepMap 100 Å, 75 um × 2 cm) and peptide separation was performed using an EASY-Spray C18 reversed-phase nano LC column (PepMap RSLC C18, 2 um, 100 Å, 75 um × 25 cm). A linear gradient of 6 to 40% buffer B (0.1% FA in ACN) against buffer A (0.1% FA in water) during 78 min and 100% buffer B against buffer A till 100 min, was carried out with a constant flow rate of 300 nl/min. Full scan MS spectra were recorded in the positive mode electrospray ionization with an ion spray voltage power frequency (pf) of 1.9 kV (kV), a radio frequency lens voltage of 60 and a capillary temperature of 275 °C, at a resolution of 30,000 and top 15 intense ions were selected for MS/MS under an isolation width of 1.2 m/z units. The MS/MS scans with higher energy collision dissociation fragmentation at normalized collision energy of 27% to fragment the ions in the collision induced dissociation mode.

Peptide and protein identification and quantification

Proteome Discoverer (v2.1, Thermo Fischer Scientific) was used for protein identification and quantification. The MS/MS spectra (.raw files) were searched by Sequest HT against the Homo sapiens UniProt database (UP000005640; 79,052 entries). A maximum of 2 tryptic cleavages were allowed, the precursor and fragment mass tolerance were 10 ppm and 0.6 Da, respectively. Peptides with a false discovery rate (FDR) of less than 0.01 and validation based on q-value were used as identified. The minimum peptide length considered was 6 and the FDR was set to 0.1. Proteins were quantified using the average of top three peptide MS1-areas, yielding raw protein abundances. Common contaminants like human keratin and bovine trypsin were also included in the database during the searches for minimizing false identifications.

Analysis of TPP experiments

Melting curves were calculated using a sigmoidal fitting approach with the R package TPP, as described in[6], with modifications. The fold changes were changed to correspond to the 7 temperatures, and the filter criteria for normalization were adjusted to this number of temperatures. The melting curves were fitted after normalization following the equation described in [9], computed in R:

$$f(T) = \frac{1 - plateau}{1 + e^{-\left(\frac{a}{T} - b\right)}} + plateau$$

where *T* is the temperature, and a, b and "plateau" are constants. The value of f(*T*) at the lowest temperature T_{min} was fixed at 1. The melting point of a protein is defined as the temperature Tm at which half of the amount of the protein has been denatured. The quality criteria for filtering the sigmoidal melting curves were: (i) fitted curves for both vehicle- and compound-treated conditions had an R^2 of >0.8; (ii) the vehicle curve had a plateau of <0.3; (iii) the melting point differences under both the control and the treatment conditions were greater than the melting point difference between the two controls; and (iv) in each biological replicate, the steepest slope of the protein melting curve in the paired set of vehicle- and compound-treated conditions was below −0.06. The NPARC of the R package was used to detect significant changes in the temperature-dependent melting behavior of each protein due to changes in experimental conditions[6]. The significance threshold was set at $p < 0.05$.

Surface plasmon resonance (SPR)

The binding of WASP and EG-011 was investigated by surface plasmon resonance. A construct corresponding to the WH1 and GBD-C region was expressed and purified by Genescript. The protein was immobilized by aminocoupling on a CM5 chip dissolving it in acetic buffer at pH 4.5.
Five increasing concentrations of EG-011 18.12, 36.25, 72.5, 150, 300 mM were injected using a single-cycle kinetics setting. PBS containing 2% of DMSO to facilitate drug solubility was used as running buffer.
Subsequently, curve fitting was executed using Biacore Insight Evaluation Software (version 5.0.18).

Nuclear magnetic resonance (NMR)

To confirm binding of EG011 to the WH1 or GBD-C domain of WASP *in vitro*, we performed solution NMR analyses. We used saturation transfer difference (STD) ligand observation experiments to verify the binding of the candidate molecule to the two different WASP domains.

Pyrene actin assembly assays

Pyrene actin polymerization assays were performed with pyrene labeled actin (0.024 µg/µl, 200 µl), Arp2/3 protein complex (0.33 µg/µl, 2 µl) and WASp (0.1 µg/µl, 1 µl). Pyrene labeled actin and Arp2/3 protein complex where purchase from cytoskeleton, inc. Experiment was performed following manufactural instructions. EG-011 was dissolved in KMEI buffer (500 mM potassium chloride, 10 mM MgCl2, 10 mM EDTA, 100 mM Imidazole pH 7). Fluorescence intensity was recorded every 30 seconds, exciting at 350 nm and detecting emission at 410 nm, for a total of 75 minutes. Data are displayed as normalized fluorescence with the formula $\frac{X - X\,min}{Xmax - Xmin}$, where X = value to normalize, Xmin = minimum value of the experiment, Xmax = higher value in the experiment.

Immunofluorescence

After treatment, cells were allowed to attach to poly-L-lysine coated slides and then fixed for 20 min with PFA 4% at room temperature (RT). Cells were permeabilized with PBS + 0.1% Triton X-100 10min at RT. To avoid unspecific staining, samples were blocked for 1 hour with PBS + 5% BSA at RT before staining. To stain F-actin we used Alexafluor-488-phalloidin (Fluorescein Phalloidin, Invitrogen, US). Samples were incubated 45 min at RT. Slides were counterstained after 3 washes of PBS with 0.3 µg/mL 4,6-diamidino-2-phenylindole (DAPI) (Sigma-Aldrich). Cells were treated the same way to stain for activated WASp but immunostained

following fixing, permeabilizing, and blocking described above. Antibodies were diluted in PBS + 5% BSA. The primary anti-"active WASp" antibody was used at 1:100 dilution. Samples were incubated overnight at 4°C. Then, samples were washed with PBS + 1% BSA and stained with a 1:1000 dilution of AlexaFluor-488 labeled goat anti-mouse secondary antibody (ab150113, Abcam, UK). Images for fluorescence intensity analysis were acquired on a widefield Nikon Eclipse E800 microscope with a 20x objective (NA 0.75). GFP and DAPI filter were used, excitation with Lumencor SOLA LED light, and image acquisition with NIKON DS FI3 camera. Two images of more than 100 cells each were analyzed for each biological replicate. The representative images shown were acquired using a confocal microscope Leica tcs sp5. Objective HCX PL APO lambda blue, 63X/NA 1.4, oil immersion objective was used. Pixel size 80.1 nm. Excitation was performed with 405 nm diode laser and argon laser (488 nm), with collection in ranges 380-493 nm and 493-655 nm, respectively. Analysis was performed with ImageJ software. Briefly, images were converted into grayscale. ROI was selected using a threshold of pixel intensity of 5 and 15 for mean fluorescence intensity.

Cellular PK of EG-011

Intra and extracellular concentrations of EG-011 analysis were done as follow. Cells were seeded at 1x106 cells/mL and exposed to 96.5 ng/mL (0.2 µM) EG-011 for 0, 5, 15, 30, 60, 120 and 360 min. At each time point, cells were collected and centrifuged at 2000 rpm for 5 minutes at 4C. Supernatant (5 mL) was collected, and the cell pellet was washed with PBS and stored at -20C. EG-011 extracellular and intracellular concentrations were analyzed in cell supernatants and pellets, respectively, using Ultra Performance Liquid Chromatography with tandem mass spectrometry.

Metabolic stability

The assay was performed with hepatocytes from CD-1 mouse (male, TPCS), Sprague-Dawley rat (male, BioIVT), Beagle dog (male, BioIVT) and pooled human (BioIVT). EG-011 was tested at 1 µM with a final hepatocyte concentration of 1 million cells/mL. Reaction mixtures were incubated for up to 120 min at 37°C in a CO2 incubator at 100 rpm. At each time points (0, 30, 60, 90 and 120 min), reaction mixtures were removed and terminated by acetonitrile containing internal standard. After centrifugation, supernatants were analyzed by AB SCIEX QTrap 4500/QTrap 4000/API4000. Equation of first order kinetics was used to calculate t1/2 and Clint via Microsoft Excel.

Mouse pharmacokinetic

Following EG-011 treatment (IP 200 mg/kg & PO 200 mg/kg), male BALB/c mice were serially bleeding (5, 15, 30, 60, 120, 240 and 360 min), blood was collected, plasma was separated and deproteinized. Following EG-011 treatment (PO 200 mg/kg, dosed 30 min after PO administration of 50 mg/kg ketoconazole), male BALB/c mice were bled (5, 15, 30, 60, 120, 240, 360 and 480 min), blood was collected, plasma was separated and deproteinized. The protein free supernatant diluted 3x with MeOH:H2O (1:1, v:v, with 0.1% FA) was analyzed using a quadrupole LC/MS/MS spectrometer (AB Sciex Triple Quad 5500). Data collection was performed using Analyst Software versions 1.6.3 including linear regression with weighting 1 / (x * x) was performed using the same software. Phoenix WinNonlin Software (version 8.0) was used to run pharmacokinetic analysis.

EG-011 analogue synthesis

A solution of (±)-1-[(4-phenoxyphenyl)methyl]-3-(3-piperidyl)pyrido[3,2-*d*]pyrimidine-2,4-dione (114 mg, 0.27 mmol) in dry DCM (2 mL) was cooled at 0 °C. TEA (0.11 mL, 0.79 mmol) and propionyl chloride (0.03 mL, 0.30 mmol) were added to the solution. The mixture was left to react at room temperature for 5 h, after which additional dry DCM (1 mL), TEA (0.4 mL, 0.29 mmol) and propionyl chloride (0.01 mL, 0.10 mmol) were added. The reaction was left to react overnight at room temperature, diluted with DCM and washed with 5% aqueous citric acid. The aqueous layer was extracted with DCM and the combined organic layers were washed with brine, dried over sodium sulfate and filtered. The solvent was evaporated and the residue was purified using silica column chromatography (DCM to DCM:MeOH = 97 : 3) to give the final compound as a white solid after repeated evaporation with diethyl ether (56 mg, 0.12 mmol, 43% yield). MS/ESI$^+$ 484.95 $[MH]^+$, Rt = 13.0 min; ^{1}H NMR (400 MHz, DMSO-d_6) δ ppm 8.53 (td, 1H), 7.71 - 7.77 (m, 1H), 7.67 (dt, 1H), 7.33 - 7.43 (m, 4H), 7.09 - 7.16 (m, 1H), 6.92 - 7.02 (m, 4H), 5.25 - 5.40 (m, 2H), 4.68 - 4.85 (m, 1H), 4.40 - 4.54 (m, 1H), 3.43 - 4.01 (m, 2H), 2.52 - 3.00 (m, 2H), 2.25 - 2.40 (m, 2H), 1.72 - 1.89 (m, 2H), 1.34 - 1.59 (m, 1H), 1.01 (t, 3H).

Supplementary Results

Chemical synthesis

1-[(4-phenoxyphenyl) methyl]-3-(1-prop-2-enoyl-3-piperidyl) pyrido [3, 2-d] pyrimidine-2, 4-dione, namely EG-011 was chemical synthesized by Chimete by following a scheme reported in the Figure 1C.

Step 1: synthesis of methyl 3-[(1-tert-butoxycarbonyl-3-piperidyl)carbamoylamino] pyridine-2-carboxylate

To a solution of methyl 3-isocyanatepyridine-2-carboxylate (prepared as described in Synthetic Communications, 2003, 33(24), 4259-4268; 1.20 g, 6.736 mmol) in dry dichloromethane (8 mL), a solution of racemic tert-butyl 3-aminopiperidine-1- carboxylate (1.349 g, 6.736 mmol) in DCM (4 mL) was added drop-wise and the resulting mixture was stirred at room temperature overnight. After evaporation of the solvent at reduced pressure, the residue was purified by flash chromatography on Biotage KP-Sil SNAP cartridge (DCM : EtOAc = 80 : 20 to 100% EtOAc). A further purification by flash chromatography on Bitotage NH SNAP cartridge (hexane : EtOAc = 80 : 20 to 40 : 60) was required to afford title compound (1.4 g). MS/ESI+ 379.1 [MH]+, Rt = 13.6 min

Step 2: synthesis of tert-butyl 3-(2,4-dioxo-1H-pyrido[3,2-d]pyrimidin-3-yl)piperidine- 1-carboxylate.

To a solution of methyl 3-[(1-tert-butoxycarbonyl-3 piperidyl)carbamoylamino]pyridine-2-carboxylate (1.3 g) in MeOH (15 mL), 20% sodium ethoxide solution in EtOH (1.48 mL, 3.8 mmol) was added and the resulting mixture was heated to reflux for 8 h, then stirred at room temperature overnight. The mixture was evaporated to dryness together with a smaller batch (obtained by reacting 0.100 g of methyl 3-[(1-tert-butoxycarbonyl-3-piperidyl)carbamoylamino]pyridine-2-carboxylate under the same conditions) and the residue was dissolved in water and acidified with acetic acid (pH ≈ 4-5). The precipitate was collected by filtration and washed several times with plenty of water.

The solid was dried under vacuum at 50°C affording title compound as a beige solid (1.1 g, 3.175 mmol, 47% yield over 2 steps). MS/ESI+ 347.0 [MH]+, Rt = 11.8 min

Step 3: synthesis of tert-butyl 3-[2,4-dioxo-1-[(4-phenoxyphenyl)methyl]pyrido[3,2- d]pyrimidin-3-yl]piperidine-1-carboxylate.

To a suspension of tert-butyl 3-(2,4-dioxo-1H-pyrido[3,2-d]pyrimidin-3-yl)piperidine-1-carboxylate (1.00 g, 2.89 mmol) in dry DMF (8 mL), K_2CO_3 (0.798 g, 5.78 mmol) was added followed by a solution of 1-(bromomethyl)-4-phenoxy-benzene (0.911 g,3.46 mmol) in DMF (1 mL) and the resulting mixture was stirred at room temperature for 46 h. The mixture was partitioned between EtOAc (70 mL) and water (60 mL). The organic phase was washed with brine (3 x 70 mL), dried over sodium sulfate, filtered and concentrated. The residue was purified by flash chromatography on Biotage KP-Sil SNAP cartridge (100% EtOAc) to afford title compound as a beige foam (1.380 g, 2.61 mmol, 90% yield). MS/ESI+ 529.1 [MH]+, Rt = 25.4 min

Step 4: synthesis of 1-[(4-phenoxyphenyl)methyl]-3-(3-piperidyl)pyrido[3,2-d]pyrimidine-2,4-dione

To a solution of tert-butyl 3-[2,4-dioxo-1-[(4-phenoxyphenyl)methyl]pyrido[3,2- d]pyrimidin-3-yl]piperidine-1-carboxylate (1.375 g, 2.60 mmol) in DCM (20 mL) cooled to 3°C, TFA (1.992 mL, 26.0 mmol) was added drop-wise and the resulting mixture was left to warm to r.t. and stirred for 6 h. The mixture was diluted with DCM and washed with sat. $NaHCO_3$. The organic phase was dried over sodium sulfate, filtered and concentrated to afford title compound as a beige foam (1.086 g, 2.53 mmol, 97% yield) which was used without purification. MS/ESI+ 429.0 [MH]+, Rt =8.9 min

Step 5: synthesis of 1-[(4-phenoxyphenyl)methyl]-3-(1-prop-2-enoyl-3- piperidyl)pyrido[3,2-d]pyrimidine-2,4-dione

A solution of 1-[(4-phenoxyphenyl)methyl]-3-(3-piperidyl)pyrido[3,2-d]pyrimidine- 2,4-dione (1.08 g, 2.52 mmol) and TEA (1.054 mL, 7.56 mmol) in DCM (20 mL) was cooled to 3°C and acryloyl chloride (0.246 mL, 3.02 mmol) was added. The mixture was left to warm to room temperature (RT). and stirred overnight. The mixture was diluted with DCM and washed with 5% aqueous citric acid. The aqueous phase was extracted with DCM and the combined organic layers were washed with brine, dried over sodium sulfate, filtered and concentrated. The residue was purified by flash chromatography on Biotage KP-Sil SNAP cartridge (DCM to DCM : MeOH = 95 : 5). A further purification by flash chromatography on Biotage Ultra silica SNAP cartridge (EtOAc to EtOAc:MeOH = 95 : 5) was required to afford title compound as white foam (0.640 g, 1.326 mmol, 53% yield). MS/ESI+ 483.1 [MH]+, Rt = 17.4 min; 1H NMR (300 MHz, DMSO- d6) δ ppm 8.54, (d, 1 H), 7.60 - 7.85 (m, 2 H), 7.27 - 7. 50 (m, 4 H), 7.13 (t, 1 H), 6.65- 7.05 (m, 5 H), 6.14 (d, 1 H), 5.69 (d, 1 H), 5.20 - 5.48 (m, 2 H), 4.71 - 4.88 (m, 1H), 4.40 - 4.65 (m, 1 H), 4.05 - 4.260 (m, 1 H), 3.50 - 4.05 (m, 1 H), 2.35 - 3.15 (m, 2 H), 1.77 - 1.95 (m, 2 H), 1.34 - 1.62 (m, 1 H).

References

1. Chou TC. Drug combination studies and their synergy quantification using the Chou-Talalay method. Cancer Res. 2010;70(2):440-446.
2. Meyer CT, Wooten DJ, Paudel BB, et al. Quantifying Drug Combination Synergy along Potency and Efficacy Axes. Cell Syst. 2019;8(2):97-108 e116.
3. Frismantas V, Dobay MP, Rinaldi A, et al. Ex vivo drug response profiling detects recurrent sensitivity patterns in drug-resistant acute lymphoblastic leukemia. Blood. 2017;129(11):e26-e37.
4. Ritz C, Baty F, Streibig JC, Gerhard D. Dose-Response Analysis Using R. PLoS One. 2015;10(12):e0146021.
5. Ullman-Culleré MH, Foltz CJ. Body condition scoring: a rapid and accurate method for assessing health status in mice. Lab Anim Sci. 1999;49(3):319-323.
6. Franken H, Mathieson T, Childs D, et al. Thermal proteome profiling for unbiased identification of direct and indirect drug targets using multiplexed quantitative mass spectrometry. Nat Protoc. 2015;10(10):1567-1593.
7. Smith PK, Krohn RI, Hermanson GT, et al. Measurement of protein using bicinchoninic acid. Anal Biochem. 1985;150(1):76-85.
8. Wisniewski JR, Zougman A, Nagaraj N, Mann M. Universal sample preparation method for proteome analysis. Nat Methods. 2009;6(5):359-362.
9. Savitski MM, Reinhard FB, Franken H, et al. Tracking cancer drugs in living cells by thermal profiling of the proteome. Science. 2014;346(6205):1255784.
10. Arribas AJ, Napoli S, Cascione L, et al. Resistance to PI3Kdelta inhibitors in marginal zone lymphoma can be reverted by targeting the IL-6/PDGFRA axis. Haematologica. 2022;107(11):2685-2697.
11. Arribas A, Napoli S, Cascione L, et al. Secondary resistance to the PI3K inhibitor copanlisib in marginal zone lymphoma. Eur J Cancer. 2020;138(S40-S40.
12. Arribas AJ, Napoli S, Gaudio E, et al. Abstract A127: Secretion of IL16 is associated with resistance to ibrutinib in pre-clinical models of lymphoma. Mol Cancer Ther. 2019;18(12_Supplement):A127-A127.
13. Arribas AJ, Napoli S, Cascione L, et al. ERBB4-Mediated Signaling Is a Mediator of Resistance to PI3K and BTK Inhibitors in B-cell Lymphoid Neoplasms. Mol Cancer Ther. 2024;23(3):368-380.

Supplementary Figures

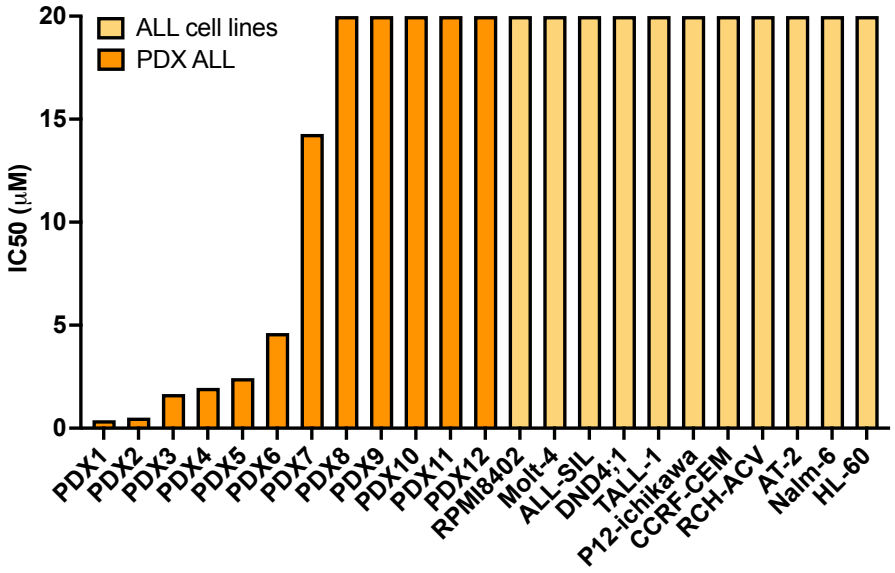

Histology	Cell lines
T-ALL	RPMI8402
T-ALL	Molt-4
T-ALL	ALL-SIL
T-ALL	DND4;1
T-ALL	TALL-1
T-ALL	P12-ichikawa
T-ALL	CCRF-CEM
B-ALL	RCH-ACV
B-ALL	AT-2
B-ALL	Nalm-6
promyelocytic leukaemia	HL-60

Supplementary figure 1. EG-011 activity in ALL PDX and cell lines. EG-011 in vitro activity in ALL PDX and ALL cell lines. Each dot represents a PDX or a cell line with the respective IC50 calculated with proliferation assay after 72h of treatment. IC50 >10 μM, arbitrary set as 20 μM. On the right, table with the list of ALL cell lines with the respective histology.

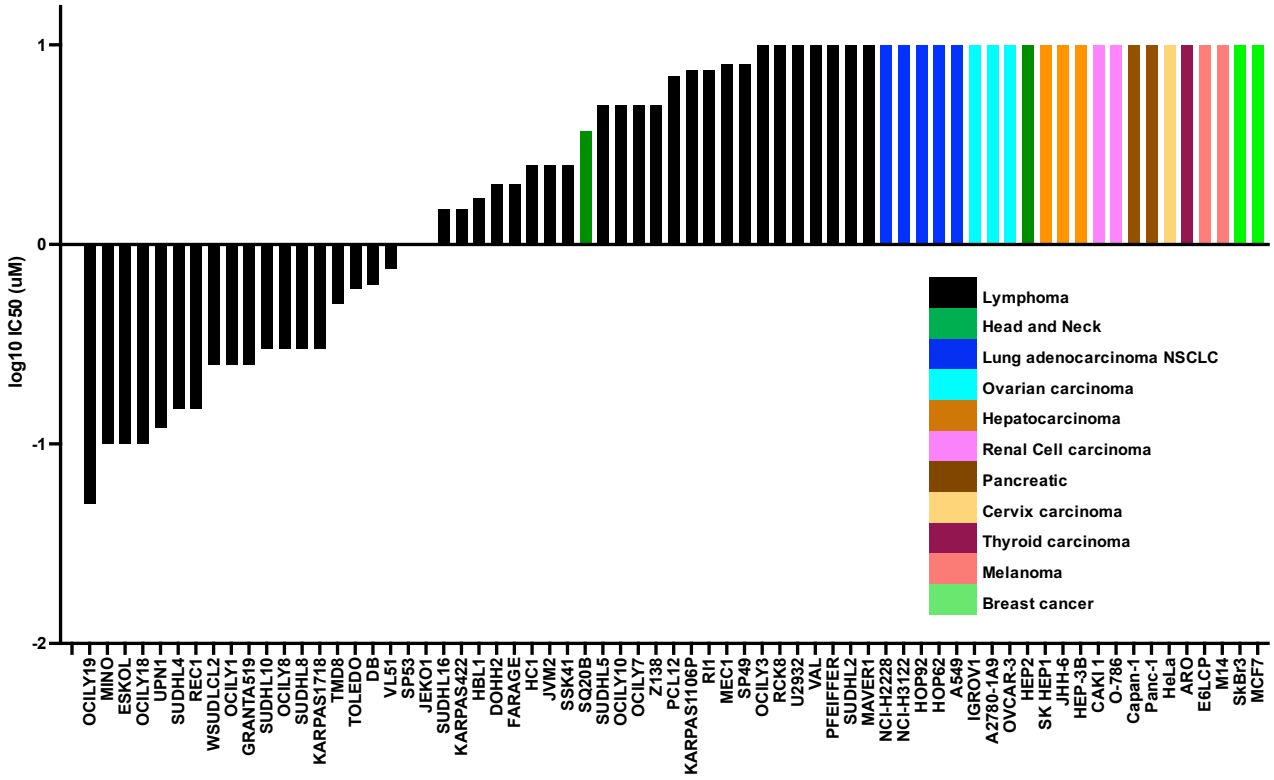

Supplementary Figure 2. EG-011 has anti-tumor activity only in hematological cancers. EG-011 in vitro activity in lymphoma cell lines and solid tumor cell lines. IC50s calculated after 72h of treatment. IC50 >10 μM, arbitrary set as 20 μM.

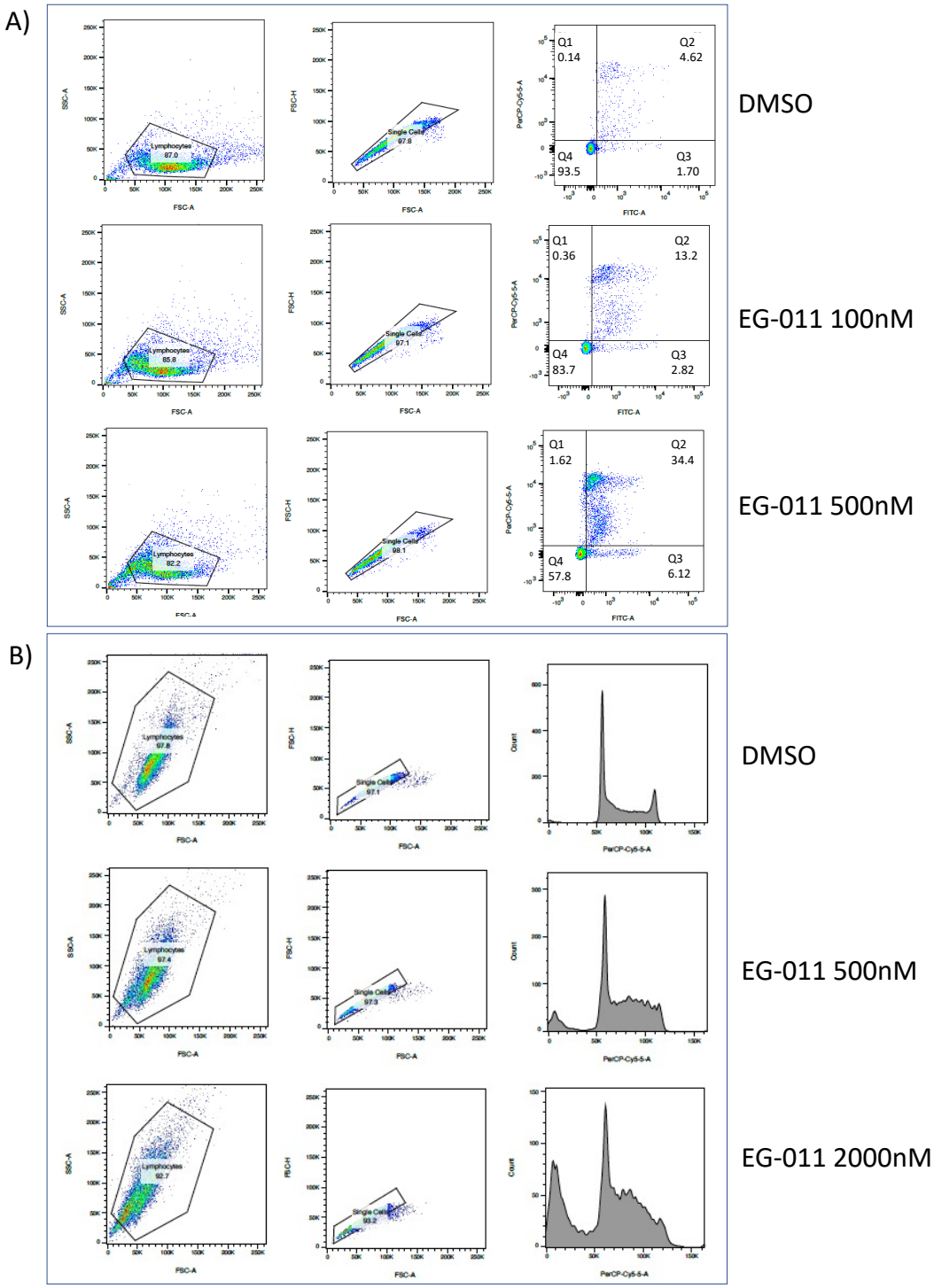

Supplementary Figure 3. EG-011 induces cell death. A) Representative images of flow cytometry apoptosis/annexin V experiment in OCILY19 treated with EG-011 for 72h. Q4: living cells. Q2 and Q3: apoptotic cells. B) Representative images of flow cytometry cell cycle experiment in OCILY19 treated with EG-011 for 72h.

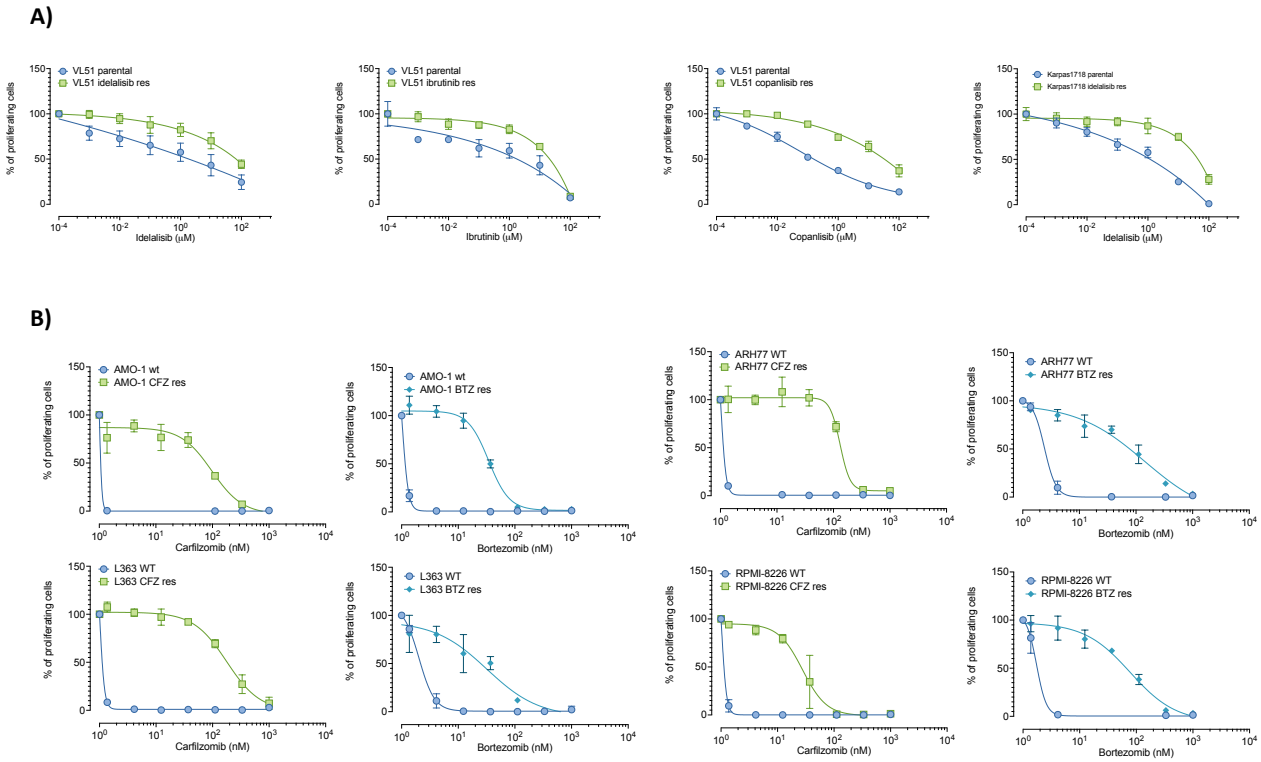

Supplementary Figure 4. Marginal zone lymphoma (MZL) and multiple myeloma (MM) models with acquired resistance to FDA-approved compounds. A) Dose-response curves after 72h treatment with idelalisib, ibrutinib, or copanlisib in MZL cell lines with acquired resistance to PI3K and BTK compared to parental cells. **B)** Dose-response curves after 72h treatment with carfilzomib (CFZ) and bortezomib (BTZ) in MM cell lines with acquired resistance to proteasome inhibitors compared to parental cells. Raw data for MZL cell lines treated with PI3K and BTK inhibitors were already published and were re-analyzed for the figure [10-13].

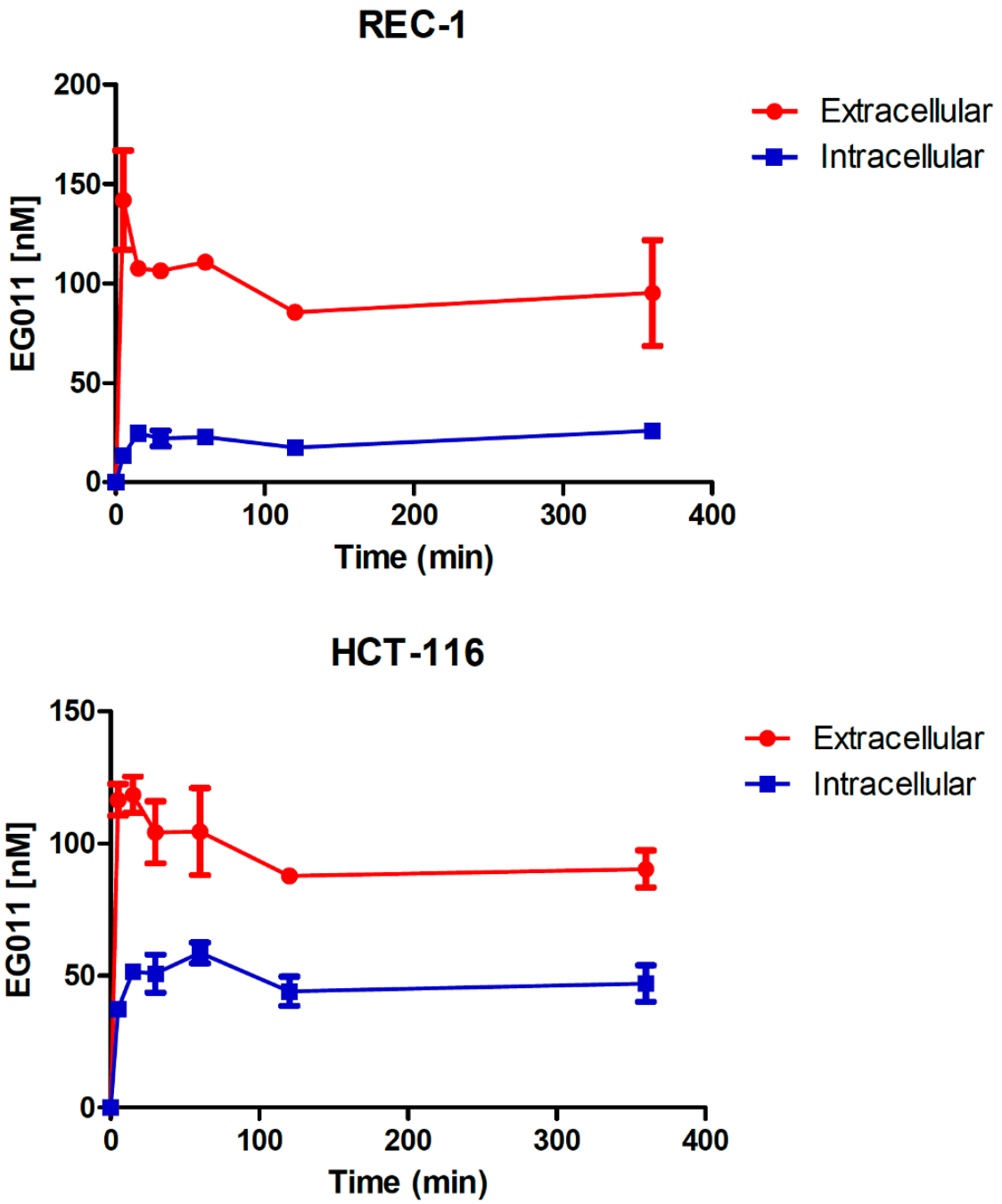

Supplementary Figure 5. Differences in cellular uptake do not explain the lack of activity in solid tumors. Extracellular and intracellular levels of EG-011 analyzed over time in the solid tumor resistant model HCT-116 (colorectal cancer cell line) and in the lymphoma sensitive model cell line REC1 (MCL cell line).

L1000

Drug	MOA	NES
Nsc-632839	ubiquitin specific protease inhibitor	2.3529
Scriptaid	HDAC inhibitor	2.3327
Entinostat	HDAC inhibitor	2.2736
Nsc-3852	HDAC inhibitor	2.2619
Belinostat	HDAC inhibitor	2.2492
Dacinostat	HDAC inhibitor	2.2391
Cd-437	retinoid receptor agonist	2.2268
Tw-37	BCL inhibitor	2.2125
Bibr-1532	telomerase inhibitor	2.2087
Bortezomib	proteasome inhibitor	2.2029
Trichostatin-A	HDAC inhibitor	2.1987
Cerulenin	fatty acid synthase inhibitor	2.1744
Tg-101348	FLT3 inhibitor|JAK inhibitor	2.1508
Pyroxamide	HDAC inhibitor	2.143
Panobinostat	HDAC inhibitor	2.1384
Vorinostat	HDAC inhibitor	2.1374
Doxorubicin	topoisomerase inhibitor	2.136
Ikk-2-Inhibitor-V	IKK inhibitor| NFkB pathway inhibitor	2.1319
Gw-405833	cannabinoid receptor agonist	2.1267
Mg-132	proteasome inhibitor	2.1263
Menadione	mitochondrial DNA polymerase inhibitor	2.1155
Nsc-663284	CDC inhibitor	2.0998
Serdemetan	MDM inhibitor	2.0937
Perhexiline	carnitine palmitoyltransferase inhibitor	2.0845
Ryuvidine	histone lysine methyltransferase inhibitor	2.0783
Cladribine	adenosine deaminase inhibitor	2.0777
Tyrphostin-Ag-1478	EGFR inhibitor	2.0583
Ikk-16	IKK inhibitor	2.0467
Tyrphostin-A9	tyrosine kinase inhibitor	2.042
Bi-2536	PLK inhibitor	2.0369
Sn-38	topoisomerase inhibitor	2.0359
Elesclomol	oxidative stress inducer	2.0358
Purvalanol-A	CDK inhibitor	2.0322
Pac-1	caspase activator	2.029
Cd-1530	retinoid receptor agonist	2.028
Etoposide	topoisomerase inhibitor	2.0273
Quiflapon	leukotriene synthesis inhibitor	2.0174
Bx-795	IKK inhibitor	2.0173
Calcipotriol	vitamin D receptor agonist	1.9915

GDSC

Drug	MOA	NES
Docetaxel	Microtubulin-stabilizing agent	2.1683
CGP-60474	Cell Cycle (Interphase), Mitosis	2.0369
SL 0101-1	ERK Signalling, Mitosis	2.0212
Bortezomib	proteasome inhibitor	1.9013
TGX221	NA	1.8931
Epothilone B	Microtubulin-stabilizing agent	1.8819
JNK Inhibitor VIII	Stress Pathways	1.8689
BIBW2992	ERK Signalling, PI3K/MTOR	1.8465
BMS-509744	Adhesion, Cytoskeleton	1.8373
Gefitinib	ERK Signalling, PI3K/MTOR	1.8287
AS601245	Stress Pathways	1.8193
RO-3306	Mitosis	1.8027
Vinblastine	Microtubulin-destabilizing agent	-1.7079
ATRA	Transcription	-1.7447
MK-2206	Apoptosis, Metabolism, PI3K/MTOR	-1.7641
AZD-2281	DNA Repair, Other	-1.7972
Bosutinib	Cytoskeleton, ERK signalling, Other	-1.8322
KU-55933	DNA Repair	-1.8345
AZD7762	Cell Cycle (Interphase), DNA Repair	-1.86
Salubrinal	Other	-1.8819
Nilotinib	Cytoskeleton	-1.9032
IPA-3	Cytoskeleton,	-1.9898
AICAR	AMPK, Metabolism	-1.9951
Axitinib	Angiogenesis, ERK Signalling, PI3K/MTOR	-2.0347
PD-0332991	Cell Cycle (Interphase)	-2.0364
AP-24534	Cytoskeleton	-2.0853
LAQ824	NA	-2.0861
AZD8055	Metabolism, PI3K/MTOR	-2.1018
BX-795	Mitosis, NFkappB, PI3K/MTOR	-2.227
Vorinostat	Chromatin Modification	-2.2298
Methotrexate	Replication, Transcription	-2.2401
ZM-447439	Mitosis	-2.4763
ABT-263	Apoptosis	-2.5799

Supplementary Figure 6. EG-011 determines transcriptome changes similar to microtubule-stabilizing agents and HDAC inhibitors. Drug connectivity enrichment plots showing the compounds inducing similar or opposite transcriptional changes to REC1 cell line exposed to EG-011 treatment or to DMSO as control. Transcriptional changes induced by EG-011 treatment were compared to those induced by other drugs present in publicly available data, such as the LINCS L1000 project (L1000) and the Genomics of Drug Sensitivity in Cancer (GDSC) project.

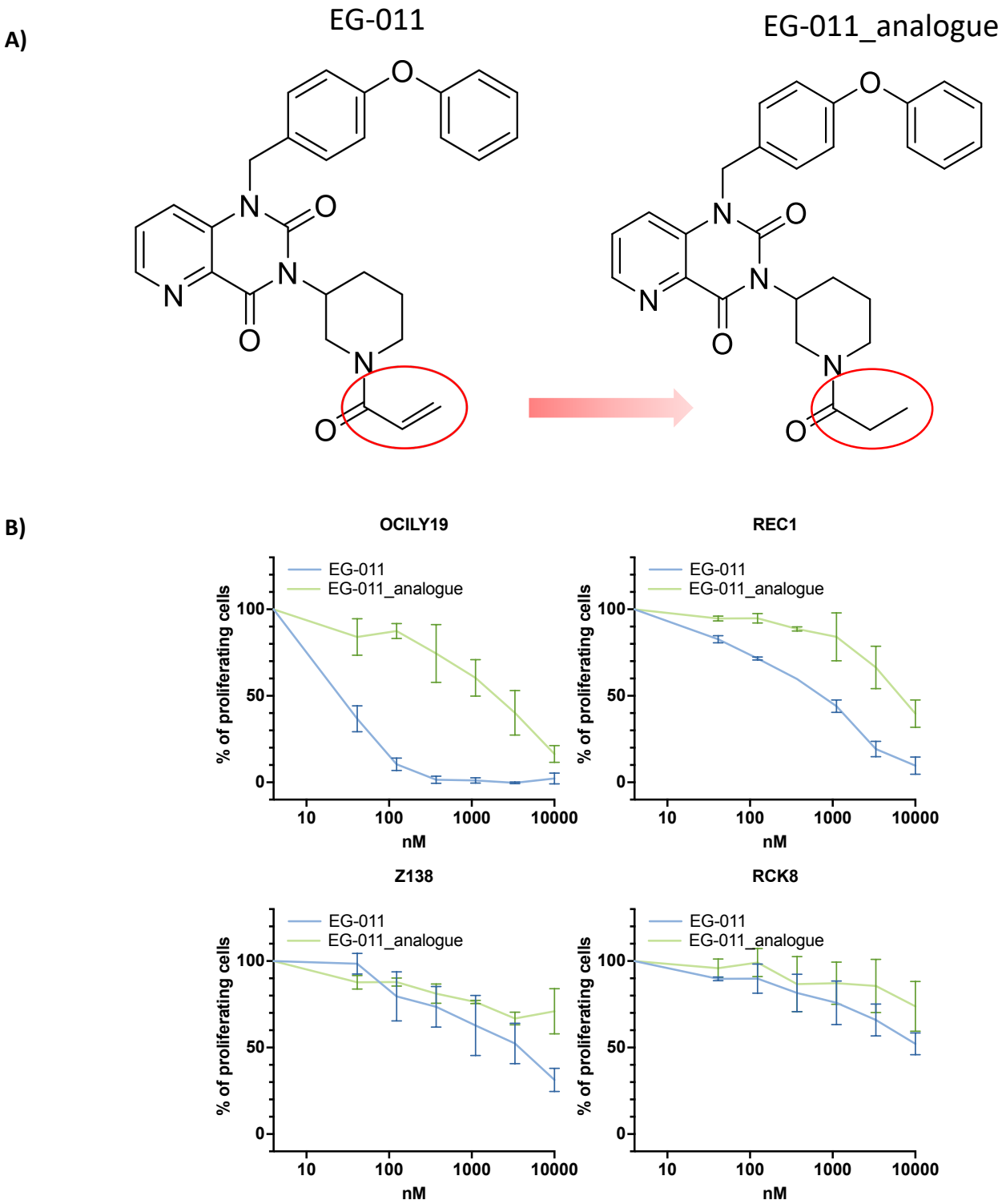

Supplementary Figure 7. EG-011 saturated analogue activity. A) Structure of EG-011 saturated analogue; in red highlighted the chemical group that was modified. **B)** Comparison of antitumoral activity between EG-011 and its saturated analogue.

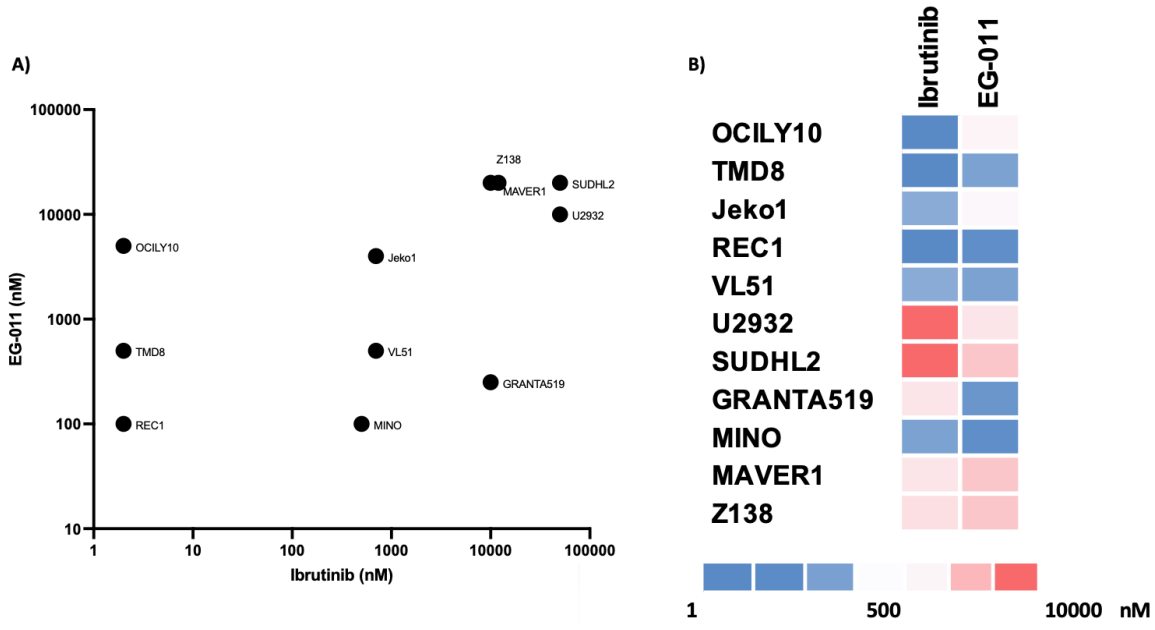

Supplementary Figure 8. EG-011 pattern of activity differs from ibrutinib. A) IC50s correlation in different lymphoma cell lines treated with EG-011 (y axis) and ibrutinib (X axis). **B**) Heatmap with EG-011 and Ibrutinib IC50s in lymphoma cell lines.

A)

Stabilized Protein

Gene name	FC Tm (Tm Treated-Tm ctr)	p-value
CUTC	2.435	0.00030
AIMP1	4.18	0.00120

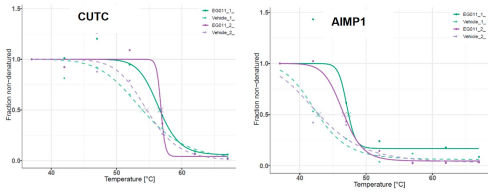

B)

Destabilized Protein

Gene name	FC Tm (Tm Treated-Tm ctr)	p-value
WAS	-12.305	0.00003
CAMK1D	-10.205	0.02700
NUDCD2	-7.125	0.01400
ELOC	-6.35	0.00100
C12orf10	-6.23	0.02300
NSUN2	-5.43	0.00800
ARHGAP25	-5.255	0.03600
SCRN1	-4.71	0.00080
PPIF	-4.7	0.01600
CCT2	-4.23	0.01700
USP14	-4.17	0.04700
GSPT1	-3.525	0.01000

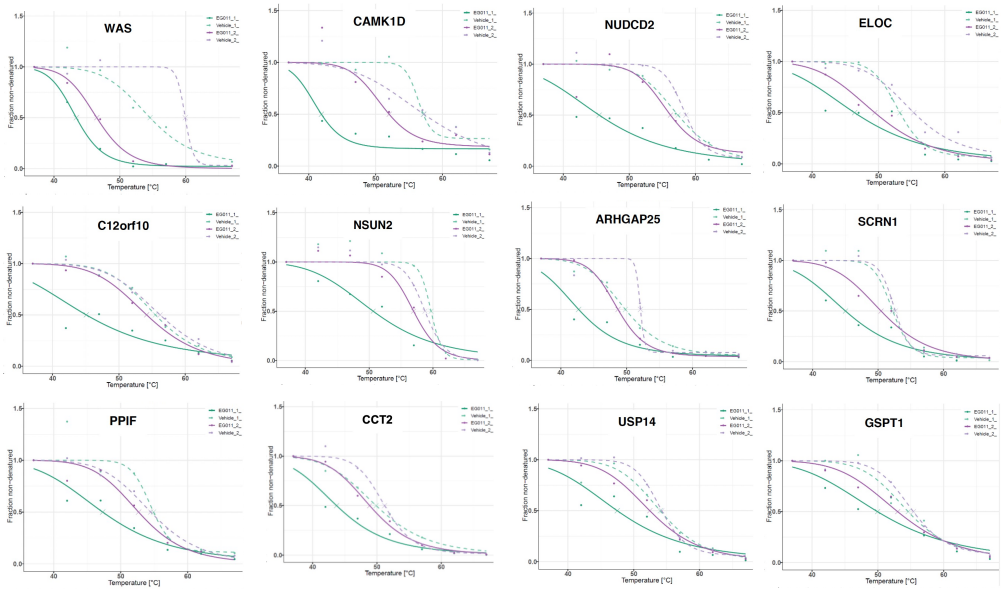

Supplementary Figure 9. Stabilized and destabilized proteins in the presence of EG-011. Statistically significantly stabilized **A)** and destabilized **B)** proteins with thermal proteomic profiling (TPP) in the presence of EG-011 or DMSO. Dashed lines, DMSO treatment; Solid lines, EG-011 treatment. Experiments performed in two replicates.

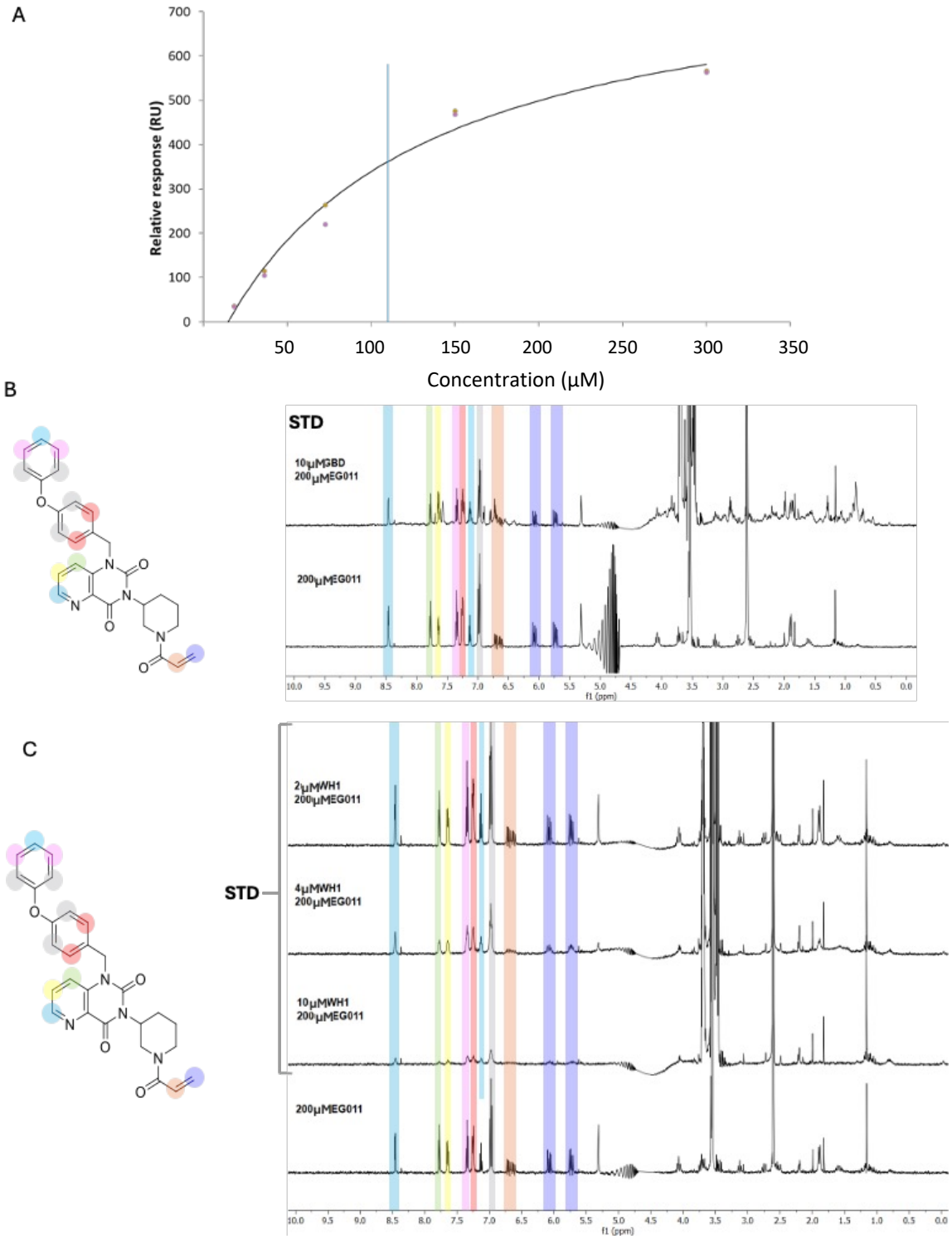

Supplementary Figure 10. Results of binding experiments. A) Surface plasmon resonance performed with immobilized WH1 WASp. Five increasing concentrations of EG-011 (18.12, 36.25, 72.5, 150, 300 µM) were injected using a single-cycle kinetics setting. Two independent experiments were performed. 1 NMR screening of compound EG011 STD experiments. Reference spectrum with most relevant assignments of **B)** 10µM GBD + 200µM EG011 and **C)** 2µM, 4µM, 10µM WH1 + 200µM EG011. The STD clearly demonstrated binding of EG-011 to the WH1 domain and a negligible effect on the GBD-C domain, comparing the two at the same concentrations. The difference spectrum of the experiment displayed distinct STD signals for most of the proton resonances of EG-011, with an effect proportional to the WH1 domain content and the most noticeable signal effect on the aromatic positions.

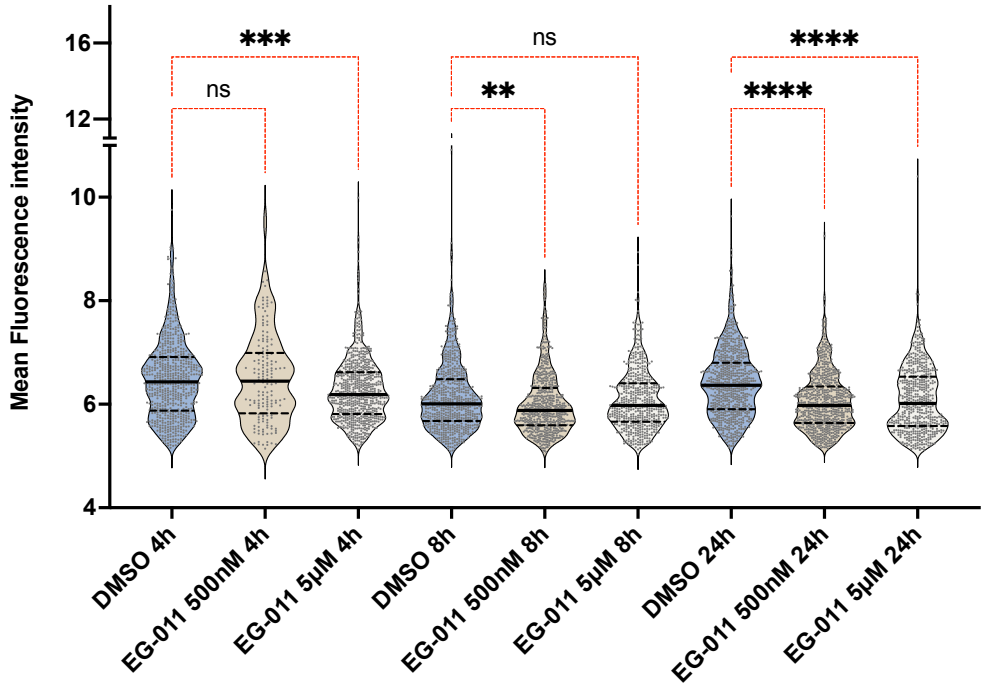

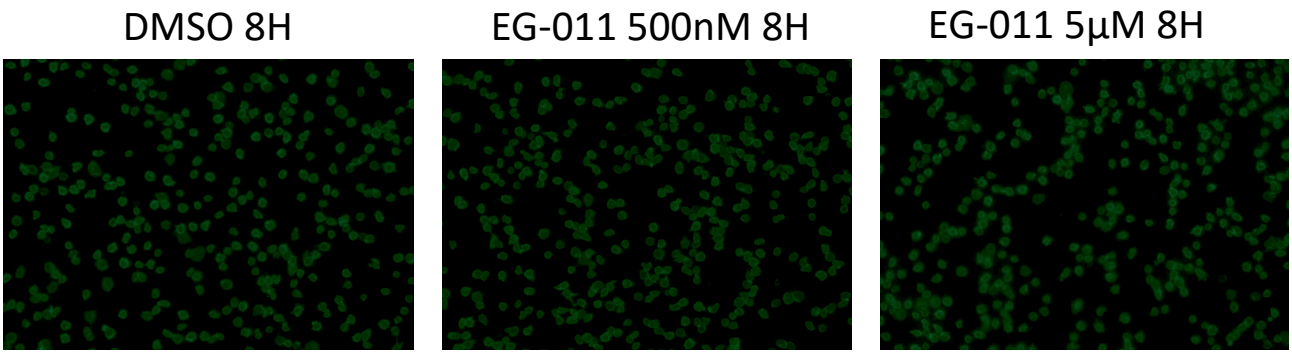

Supplementary Figure 11. Phalloidin Mean fluorescence intensity in the resistant cell line.
Phalloidin means fluorescence intensity after EG-011 treatment (500 nM and 5 µM) at 3 time points (4, 8, and 24h) compared to DMSO in resistant cell line Z138. Kruskal-Wallis test, followed by Dunn's multiple comparison, was performed. At the bottom is a representative image of fluorescence intensity. Ns = non-significant; **p<0.01; ***p<0.001; ****p<0.0001

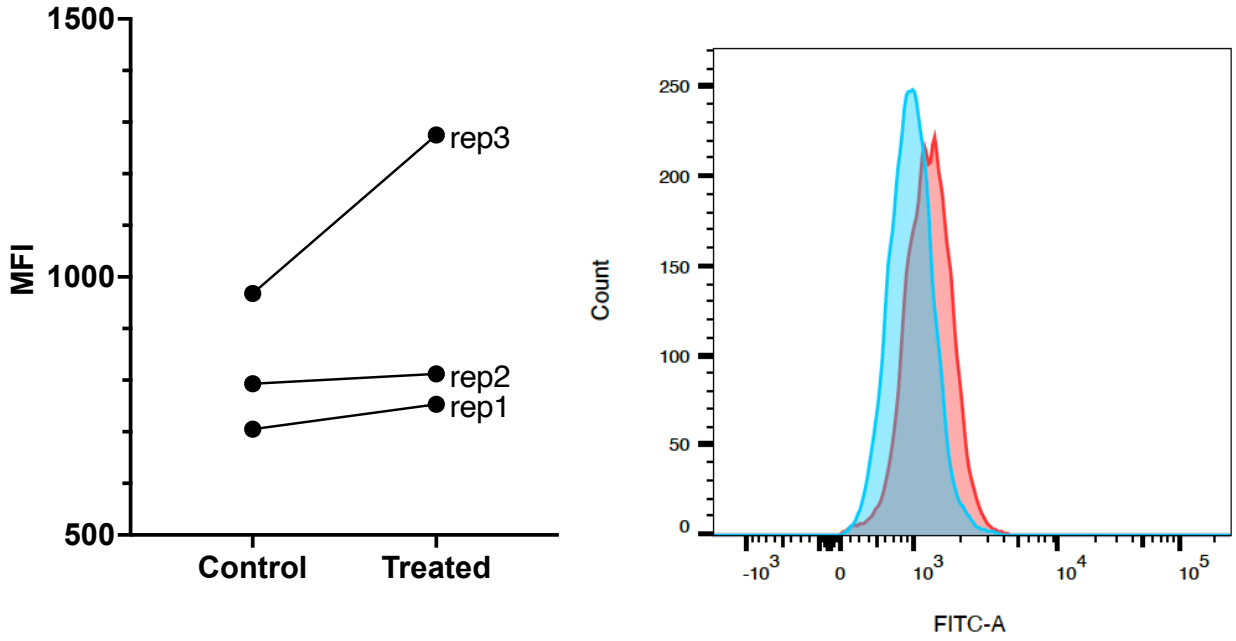

Supplementary Figure 12. Phalloidin median fluorescence intensity. FACS analysis of Phalloidin Median fluorescence intensity (MFI) increase after EG-011 long term treatment (40 nM; 3 days) compared to control in very sensitive cell lines OCILY19.

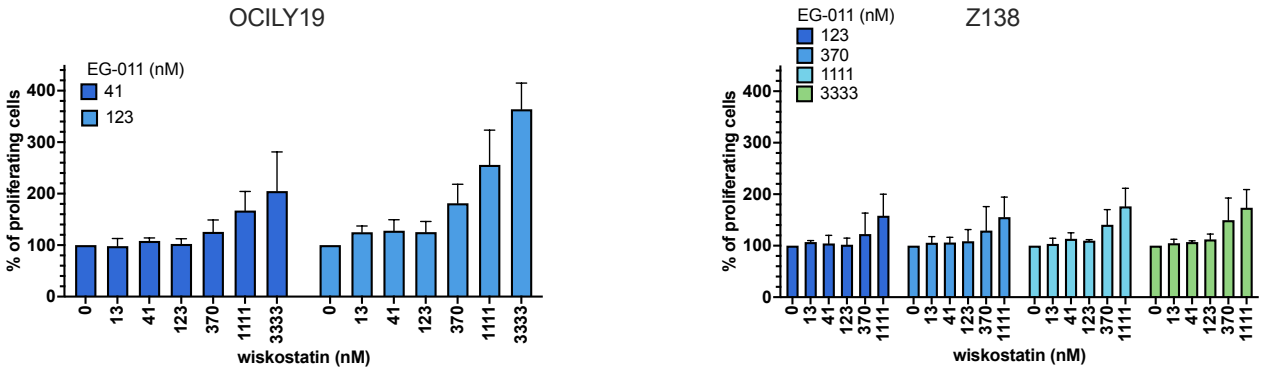

Supplementary Figure 13. EG-011 and wiskostatin combination. OCILY19 and Z138 cell lines were treated concomitantly with increasing concentrations of EG-011 and Wiskostatin. Combinations were compared to single EG-011 treatment that was set as 100%. Y-axes show the percentage of proliferating cells.

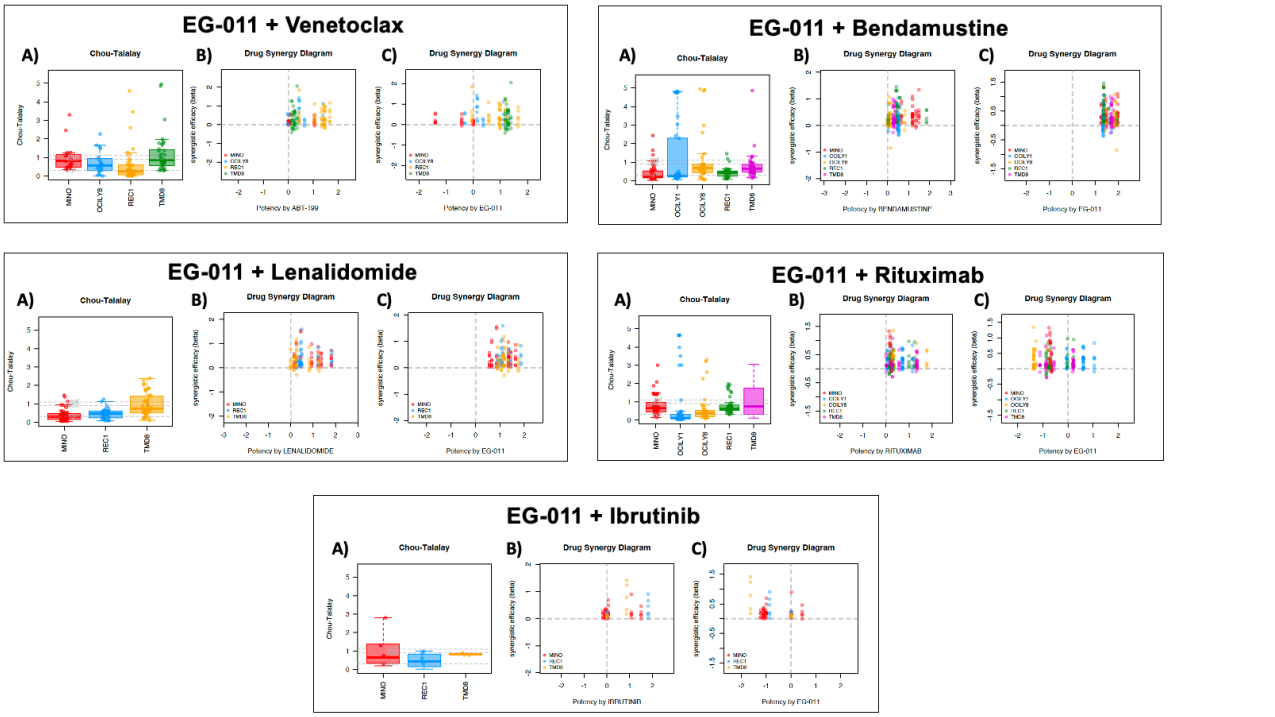

Supplementary Figure 14. EG-011 synergizes with FDA-approved compounds. Chou-Talalay index, efficacy, and potency parameters were calculated for each lymphoma cell line and each combination. In each box plot, the line in the middle of the box represents the median, and the box extends from the 25th to the 75th percentile (interquartile range, IQ); the whiskers extend to the upper and lower adjacent values (i.e., 1.5 IQ). Each point represents the CI (**A**) or efficacy and potency (**B-C**) data at the different combinations of concentrations in each cell line. Chou-Talalay Combination Index (CI): Synergism, CI < 0.9; additive effect, 0.9 < CI < 1.1; no benefit, CI >1.1. Efficacy: Synergism > 1; additive effect, from 0 to 1; no benefit from 0 to -1; antagonism < -1. Potency: Synergism > 0.5; additive effect, from 0 to 0.5; no benefit from 0 to 0.5; antagonism < -0.5

A)

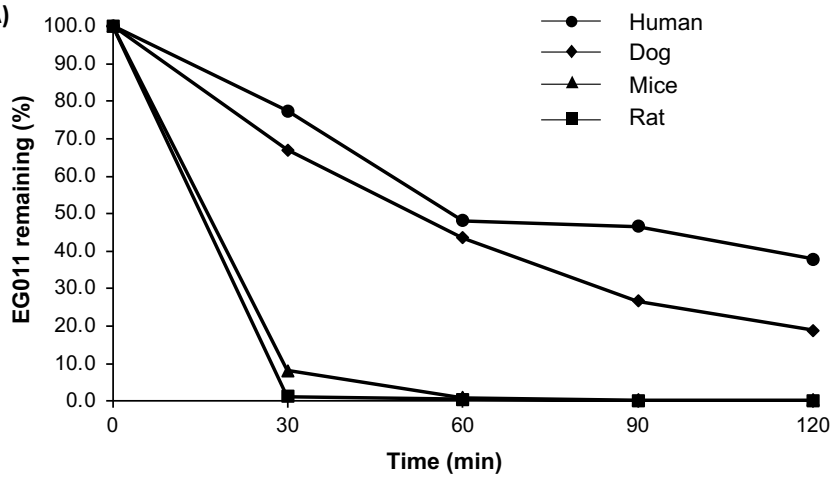

B)

Species	Mouse	Rat	Dog	Human
Time (min)	**% Remaining**	**% Remaining**	**% Remaining**	**% Remaining**
0	100,0	100,0	100,0	100,0
30	8,2	1,2	67,0	77,3
60	0,9	0,5	43,5	48,1
90	0,4	0,0	26,8	46,5
120	0,3	0,0	18,8	37,8

		7-EC (Control)			EG011		
		T1/2 (min)	**In vitro CLint (µL/min/million cells)**	**CLhep (mL/min/kg)**	**T1/2 (min)**	**In vitro CLint (µL/min/million cells)**	**CLhep (mL/min/kg)**
Species	Human	11,4	60,6	18,6	84,8	8,2	11,4
	Dog	<15.0	>46.2	>28.4	48,8	14,2	24,1
	Rat	13,1	52,8	45,3	4,7	146,9	51,2
	Mice	<15.0	>46.2	>75.9	8,3	83,5	81,6

Supplementary Figure 15. *In vitro* metabolic stability of EG011. EG-011 was incubated with multiple species of cryopreserved hepatocytes (rat, dog, mice and human; pooled) in duplicate (1 µM for five time points - 0, 30, 60, 90 and 120 min).

A)

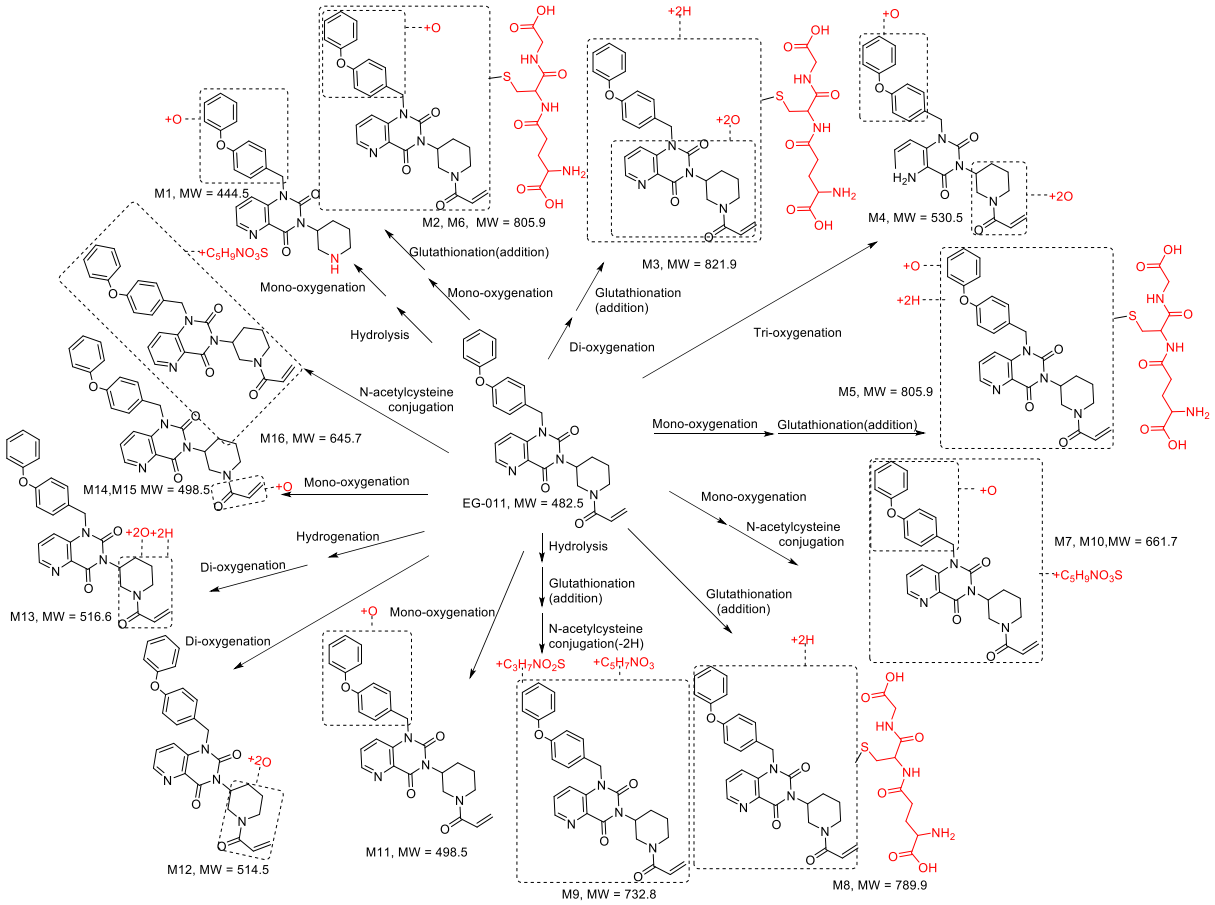

B)

Metabolite	Retention Time (min)	Theoretical *m/z* (+)	Detected *m/z* (+)	ppm	Metabolic Pathway	Relative Peak Area Abundance	
						MHep	HHep
M1	6.52	445.186	445.18	-2.2	Hydrolysis and mono-oxygenation	2.3	0.7
M2	7.08	806.280	806.27	-2.7	Mono-oxygenation and	1.4	D
M3	7.24	822.276	822.27	-2.4	Di-oxygenation and	3.0	D
M4	7.46	531.186	531.18	-1.9	Tri-oxygenation	3.3	0.8
M5	7.70	806.280	806.27	-2.2	Mono-oxygenation and	1.7	D
M6	7.81	806.280	806.27	-2.1	Mono-oxygenation and	3.4	D
M7	8.05	662.224	662.22	3.2	N-acetylcysteine conjugation and	0.2	D
M8	8.17	790.286	790.28	-3.2	glutathionation(addition)	35.1	D
M9	8.30	733.2650	733.2649	-0.1	N-acetylcysteine conjugation(-2H), glutathionation(addition) and	2.0	D
M10	8.85	662.224	662.22	1.4	N-acetylcysteine conjugation and	2.2	D
M11	8.91	499.197	499.19	-4.0	Mono-oxygenation	D	7.1
M12	9.26	515.192	515.19	-3.1	Di-oxygenation	23.5	14.5
M13	9.26	517.208	517.20	-3.3	Di-oxygenation and hydrogenation	12.8	10.8
M14	9.51	499.197	499.19	-2.2	Mono-oxygenation	0.3	0.7
M15	9.68	499.197	499.19	-2.8	Mono-oxygenation	1.3	D
M16	10.13	646.230	646.23	1.1	N-acetylcysteine conjugation	5.5	D
P(EG-011)	11.85	483.202	483.20	-1.7	--	2.0	65.4

Supplementary Figure 16. Observed Metabolites of EG-011 in Mouse and Human Hepatocytes after 120 min incubation. P, parent; D, detected; MHep, mouse hepatocytes; HHep, human hepatocytes; the relative peak area abundances of the parent and metabolites were calculated based on their selected ion chromatographic peak areas.

A)

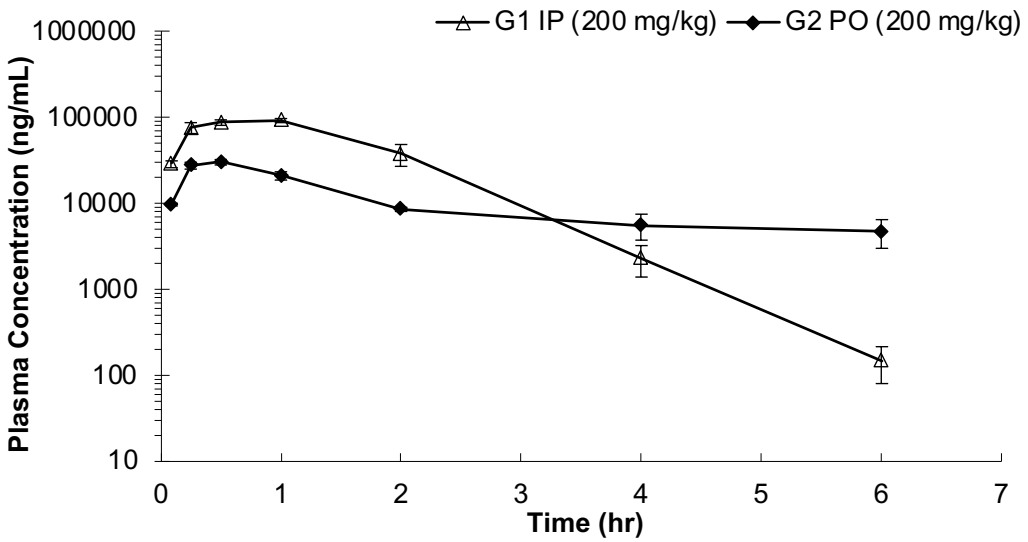

B)

EG011 IP (200 mg/kg)						
Time (hr)	**Calculated Concentration (ng/mL)**					
	Mouse #4	Mouse #5	Mouse #6	Mean	SD	CV(%)
0,0833	32100	28500	27000	29200	2621	8,98
0,25	67900	87700	73600	76400	10193	13,3
0,5	93500	80800	87900	87400	6365	7,28
1	91000	97300	89400	92567	4177	4,51
2	48300	26600	38600	37833	10870	28,7
4	2990	1280	2640	2303	903	39,2
6	223	135	90,5	150	67	45,1

EG011 PO (200 mg/kg)						
Time (hr)	**Calculated Concentration (ng/mL)**					
	Mouse #7	Mouse #8	Mouse #9	Mean	SD	CV(%)
0,0833	9520	10100	9780	9800	291	2,96
0,25	26900	30500	25400	27600	2621	9,50
0,5	32200	31300	27700	30400	2381	7,83
1	19600	23600	20100	21100	2179	10,3
2	8580	9020	8160	8587	430	5,01
4	5210	7610	3940	5587	1864	33,4
6	5070	6240	2920	4743	1684	35,5

Supplementary Figure 17. *In vivo* pharmacokinetics of EG-011. Plasma concentration data for single dose pharmacokinetic analysis of EG-011 after intraperitoneal and oral dosing (200 mg/kg).

Supplementary Table 1. List of lymphoma cell lines with relative histology and IC50 to EG-011

Supplementary Table 2. Genes and pathways modulated after EG-011 treatment.

Supplementary Table 3. List of compounds present in publicly available data of other drugs (L1000 and GDSC) with similar or opposite gene modulation to EG-011.

Supplementary Table 4. List of kinases tested as possible target of EG-011 by KINOMEscan assay PanQinase Activity Assay. Positive hits with **%** compared to CTR less then 50%.

Supplementary Table 5. List of proteins stabilized or destabilized by EG-011 identified with thermal proteome profiling.